

Mechanistic Exploration of Shugan Jianpi Formula for Treating Triple-Negative Breast Cancer Under Chronic Stress: A Network Pharmacology-Guided Experimental Study

Fen Liu^{1,*}, Luning Li^{2,*}, Yiming Zhang^{3,*}, Jiaqi Zhang², Xinchun Tian², Dengtian Zhang⁴, Ni Zhang⁵, Tinghao Yan⁵, Shulong Shi⁶, Jianlin Wu^{1,7}, Shulong Jiang^{2,3,5}

¹College of Traditional Chinese Medicine, Shandong University of Traditional Chinese Medicine, Jinan, 250000, People's Republic of China; ²Clinical Medical Laboratory Center, Jining First People's Hospital, Shandong First Medical University, Jining, 272000, People's Republic of China; ³College of First Clinical Medicine, Shandong University of Traditional Chinese Medicine, Jinan, 250000, People's Republic of China; ⁴Department of Radiation, The 960th Hospital of the PLA Joint Logistics Support Force, Jinan, 250000, People's Republic of China; ⁵Cheeloo College of Medicine, Shandong University, Jinan, 250000, People's Republic of China; ⁶Department of Endocrinology, Jining First People's Hospital, Shandong First Medical University, Jining, 272000, People's Republic of China; ⁷Key Laboratory of Traditional Chinese Medicine Classical Theory, Ministry of Education, Shandong University of Traditional Chinese Medicine, Jinan, 250000, People's Republic of China

*These authors contributed equally to this work

Correspondence: Shulong Jiang, Clinical Medical Laboratory Center, Jining First People's Hospital, Shandong First Medical University, Jining, 272000, People's Republic of China, Email jnsljiang@163.com; Shulong Shi, Department of Endocrinology, Jining First People's Hospital, Shandong First Medical University, Jining, 272000, People's Republic of China, Email 529306267@qq.com

Purpose: This study aimed to investigate the pharmacological mechanisms of Shugan Jianpi Formula (SGJPF) in treating TNBC using network pharmacology and molecular biology approaches.

Methods: HPLC/MS identified the key compounds in SGJPF. In vitro assays were performed on norepinephrine (NE)-stimulated MDA-MB-231 and SUM159PT cells to mimic triple-negative breast cancer (TNBC) under chronic psychological stress (CPS) and evaluate SGJPF's effects on cell proliferation, apoptosis, cell cycle, migration, and invasion. A TNBC mouse model exposed to CPS was used to assess SGJPF's influence on tumor growth. SGJPF's mechanisms were explored via network pharmacology and molecular docking, with target validation through Western blotting, immunohistochemistry, and immunofluorescence.

Results: HPLC/MS analysis identified 806 compounds in SGJPF, including flavonoids, polyphenols, saponins, polysaccharides, alkaloids, terpenoids, coumarins, organic acids, and glycosides. Network pharmacology and molecular docking analyses identified SRC, ERK (MAPK1), and STAT3 as pivotal targets underlying the anti-tumor effects of SGJPF in TNBC. Both in vitro and in vivo experiments confirmed that SGJPF exerts its therapeutic effects through the modulation of the SRC/ERK/STAT3 signaling axis. In vitro, SGJPF effectively inhibited TNBC cell proliferation, migration, and invasion, while promoting apoptosis in NE-stimulated cells. In a CPS-induced TNBC mouse model, SGJPF significantly alleviated tumor progression, further corroborating its potential as a novel therapeutic strategy for TNBC.

Conclusion: This study highlights the potential of SGJPF as a therapeutic strategy for TNBC through its modulation of the SRC/ERK/STAT3 signaling axis, offering a robust foundation for further investigation into its clinical application.

Keywords: Shugan Jianpi formula, triple-negative breast cancer, chronic stress, network pharmacology, SRC/ERK/STAT3 pathway

Introduction

Based on 2020 data from the International Agency for Research on Cancer (IARC), breast cancer has emerged as the most commonly diagnosed malignant tumor in women, surpassing lung cancer in new cases for the first time,¹ posing a serious threat to women's health and lives. Advances in early detection have facilitated curative treatments, including

surgery, chemotherapy, radiotherapy, and endocrine therapy. However, metastasis remains a challenge, occurring in 24%-60% of patients following surgery, particularly in triple-negative breast cancer (TNBC).² The prognosis of advanced TNBC is notably poor, with a median survival of only about 1 year. Chemotherapy is currently the standard therapeutic strategy for advanced TNBC, and how to improve overall survival and response in TNBC has become the focus of clinical attention.³

Amid accelerating global development and intensifying societal competition, chronic psychological stress (CPS), a psychiatric disorder, has been implicated in the pathogenesis and progression of TNBC.⁴⁻⁸ Patients with TNBC exhibit elevated levels of psychological stress compared to those with other cancer subtypes, owing to the aggressive nature of the disease, treatment-associated toxicities, and disruptions in family and social dynamics. These stress-related factors exert a measurable impact on clinical outcomes and overall survival. Accumulating clinical and preclinical evidence demonstrates that alleviation of CPS is beneficial to attenuate TNBC progression,⁹ suggesting CPS modulation as a potential adjunct therapeutic strategy in the management of TNBC.

It has been well established that traditional Chinese medicine (TCM) places great emphasis on the integration of psychological and physical therapy. Numerous herbal medicines and classical formulations have shown remarkable efficacy in improving both physical and mental states, positioning them as potential candidates for complementary and alternative approaches in the treatment of TNBC.¹⁰ Shugan Jianpi Formula (SGJPF), derived from the classic TCM formulation Xiaoyao Powder, exemplifies this approach. Extensive researches have confirmed the mood-stabilizing and pharmacological benefits of Xiaoyao Powder, supporting its application in the treatment of various diseases, including cancer.¹¹⁻¹⁶ Our previous clinical studies have also revealed that SGJPF can effectively delay disease progression and enhance quality of life in patients with advanced TNBC.¹⁷ In recent years, systems pharmacology and computer-aided molecular design (CAMD) have been increasingly utilized to investigate the mechanisms underlying TCM, offering powerful tools to elucidate the multi-component and multi-target interactions that characterize these therapies and contributing to the scientific advancement and modernization of TCM-based drug discovery.¹⁸

In the present study, the potential mechanism of SGJPF in treating TNBC under CPS was comprehensively explored by means of network pharmacology, molecular docking and molecular biology experiment. This study aims to provide scientific evidence supporting the application of SGJPF for TNBC treatment. The comprehensive workflow of the study is illustrated in Figure 1.

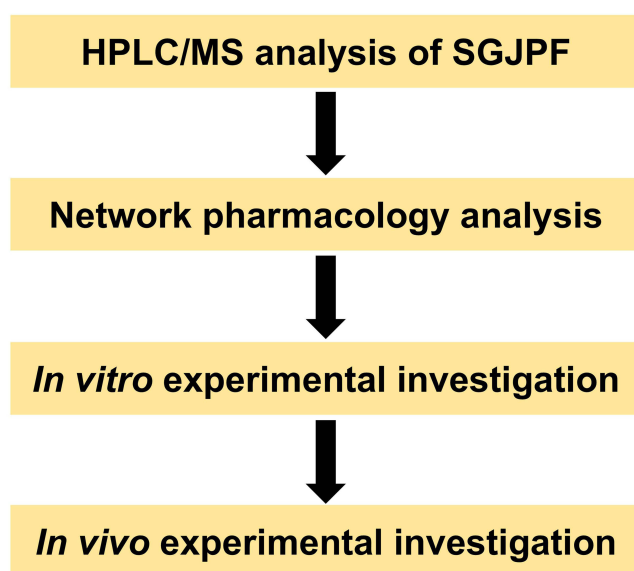


Figure 1 The flow chart of the study.

Methods

Experimental Drugs

The SGJPF is formulated with Chaihu (*Radix Bupleuri*), Baishao (*Paeoniae Radix Alba*), Shancigu (*Pseudobulbus Cremastrae Seu Pleiones*), Wuzhuyu (*Evodiae Fructus*), Guizhi (*Cinnamomi Ramulus*), Baizhu (*Atractylodes Macrocephala Koidz*), Taizishen (*Pseudostellariae Radix*), Fuling (*Poria Cocos*(Schw.) Wolf.), Juhua (*Chrysanthemi Flos*), Xiakucao (*Prunellae Spica*), Gancao (*licorice*). All raw materials involved in SGJPF were provided by Banger Chinese Herbal Decoction Pieces Co., LTD. (Jining, China). All the ingredients were soaked for 30 minutes and then mixed together for decocting. The lyophilized SGJPF powder was prepared from the crude extracts of 11 herbs according to the general preparation procedure. The concentrated liquid was spray-dried into granules, which were then sealed and stored at 4°C. For experimental use, the SGJPF powder was dissolved in culture medium and mixed thoroughly. The solution was passed through a 0.22 µm filter to sterilize it and eliminate any insoluble particles.

HPLC/MS Identified Chemical Components of SGJPF

A total of 0.15 g of SGJPF granules was weighed, followed by the addition of 1000 µL of 80% methanol and grinding beads. The mixture was ground for 5 minutes and vortexed for another 10 minutes. It was then centrifuged at 20,000 g at 4°C for 10 minutes. The supernatant obtained was collected, filtered, and subjected to computational analysis.

An electrospray ionization (ESI) source with positive/negative ion switching was used. Mass spectrometry was performed in full mass/dd-MS2 detection mode, with resolutions of 70,000 for full mass and 17,500 for dd-MS2. The scan range covered 100 to 1,500 m/z, and the electrospray voltage was set to 3.2 kV for both positive and negative modes. The capillary temperature was kept at 300°C. Nitrogen (purity ≥ 99.99%) was used as the sheath gas at a flow rate of 40 arbitrary units (Arb), while auxiliary gas flow was 15 Arb. High-purity nitrogen (purity ≥ 99.999%) served as the collision gas, with a normalized collision energy (NCE) of 30. Data were acquired over a 30-minute period.

Chromatographic separation was carried out with an AQ-C18 column (150 × 2.1 mm, 1.8 µm; Welch). The mobile phase consisted of methanol and an aqueous solution with 0.1% formic acid. The column temperature was maintained at 35°C, the sampler at 10°C, with an injection volume of 5.00 µL. Refer to [Supplementary Table 1](#) for chromatographic gradient.

Network Pharmacology

For SGJPF, the ingredients meeting the screening condition (mzCloud Best Match ≥ 70) were regarded as pharmacologically active substances.^{19,20} Then, their corresponding targets were obtained by querying SwissTargetPrediction database. The GSE38959 dataset comprises data from 30 patients with TNBC and 17 control individuals, sourced from the GPL4133-12599 platform. Microarray datasets were used to compare differentially expressed mRNAs between the control and TNBC groups, analyzed through the “limma” package in R. Genes with an adjusted p-value < 0.05 and an absolute log2 fold change > 2 were identified as differentially expressed pathogenic genes associated with TNBC. By searching the key words “chronic stress”, “anxiety” in the GeneCards database, CPS-associated known genes were identified.

The overlapping targets of SGJPF, TNBC, and CPS were considered as the therapeutic targets of SGJPF for CPS-related TNBC. Subsequently, KEGG and GO enrichment analyses were conducted with the clusterProfiler package in R. This study uses publicly available datasets, which are exempt from ethical review in accordance with Article 32, Items 1 and 2 of the Measures for Ethical Review of Life Science and Medical Research Involving Human Subjects (issued on February 18, 2023, China).

The PPI relationship of the therapeutic targets was obtained from the STRING database (<https://cn.string-db.org/>), and Cytoscape software was utilized for the integration, visualization, and analysis of biological networks. To identify the core targets, Cytohubba plugin screening, MCODE plugin filtering, and LASSO regression analysis were performed.

The structure elucidation of the identified core targets relied on data from the Protein Data Bank (PDB, <http://www.rcsb.org/>). Protein structures, stored in PDB format, were imported into AutoDockTools for molecular docking analyses. Paeoniflorin, identified as the primary active component based on previous studies and mass spectrometry results, was

selected as the ligand for docking. Its molecular structure, downloaded from the PubChem database in MOL2 format, was uploaded into AutoDockTools. Protein refinement, including the removal of original ligands and water molecules, was performed using PyMol. Binding energies were calculated using the Lamarckian genetic algorithm.

Cell Line and Culture

MDA-MB-231 and SUM159PT employed in this investigation were obtained from the Cell Bank of the Chinese Academy of Sciences (Shanghai, China) and nurtured in DMEM (Gibco, USA) supplemented with 10% fetal bovine serum (Pricella, China), 100 U/mL penicillin and 100 µg/mL streptomycin (Gibco, USA). Throughout the course of the experiment, the culture medium was maintained in an external environment at 37 °C and 5% CO₂.

Cell Viability Assay

Cell suspension (4×10^3 cells/well) was prepared and placed in 96-well plates under norepinephrine (NE) (S9507, Selleck) at a volume of 100 µL/well. After being co-cultured overnight cells were given 0.1% DMSO or different concentrations of SGJPF. Subsequently, 10 µL of CCK-8 solution (Dojindo, Japan) was introduced into each well and incubated for 1 hour. Absorbance was measured at 450 nm with a microplate reader. The IC₅₀ value was calculated to determine the optimal SGJPF intervention concentration.

Cell proliferation and DNA replication were assessed using the Edu assay kit (Ribobio, GuangDong, China). After treatment, cells were incubated in Edu staining buffer for 2 hours and then fixed with 4% paraformaldehyde. Following PBS washes, the cells were permeabilized with 0.5% Triton X-100 and stained with Apollo[®] fluorescent dye, which specifically reacts with EdU incorporated into newly synthesized DNA, allowing rapid detection of DNA replication activity. After Apollo staining, the cells were further stained with Hoechst 33342 for nuclear visualization. The stained cells were examined under a fluorescence microscope.

In the colony formation assay, cells were plated at a density of 1,000 cells per well in 6-well plates and incubated overnight. After treatment as per the experimental protocol, the cells were incubated for 14 days. Colonies were then fixed with 2 mL of methanol for 15 minutes, followed by stained with 0.1% crystal violet for an additional 15 minutes. Colony numbers were quantified using ImageJ software. All experiments were conducted in quintuplicate.

Apoptosis Analysis

Cell apoptosis was quantitatively measured through the Annexin V-APC/7-AAD apoptosis assay kit (BioGems, Suzhou, China). Cells exposed to NE were treated with SGJPF at designated concentrations for 24 hours, after which they were collected and stained with Annexin V and 7-AAD. Flow cytometer (BECKMAN, CytoFLEX, China) was used to analyze the stained cells, and the data were processed using FlowJo software (version 7.6). All experiments were conducted in quintuplicate.

Cell Cycle Analysis

MDA-MB-231 and SUM159PT cells were seeded in 6-well plates at a density of 1×10^5 cells/well, treated with NE, and exposed to different concentrations of SGJPF for 24 hours. Cells were collected with 0.25% trypsin, rinsed thoroughly with PBS, and then resuspended. The supernatant was carefully discarded after centrifugation at 1,000 g for 3–5 minutes. Subsequently, the cell pellet was gently resuspended in 1 mL of pre-cooled PBS. The cells were then fixed by incubation in 1 mL of ice-cold 70% ethanol at 4°C for 2 hours. After resuspension in pre-cooled PBS and another round of centrifugation, the cells were stained with 0.5 mL propidium iodide (PI)/RNase A solution and incubated at 37°C for 30 minutes in the dark. Following staining, each sample was analyzed by flow cytometer using a 488 nm laser. All experiments were conducted in quintuplicate.

Wound-Healing Assay

MDA-MB-231 and SUM159PT cells were inoculated into separate 6-well culture plates. Once reaching nearly 100% confluence, the monolayer cells were gently scratched using microtip tools to induce wound formation. Subsequently, the cells underwent thorough washing with PBS 2–3 times and were incubated in a serum-free medium containing with NE,

dasatinib, and varied concentrations of SGJPF. Wound healing progress was monitored, and images were taken at 0 and 24 hours with a microscope. Subsequently, the wound area was delineated for analysis using the Image J software. All experiments were conducted in quintuplicate.

Transwell Assay

Prior to the assay, the filter membrane was either coated with Matrigel (diluted 1:6) or left uncoated. MDA-MB-231 and SUM159PT cells were pre-incubated with NE and varying concentrations of SGJPF for 24 hours, then seeded into the upper chamber with serum-free medium. The lower chamber was filled with medium containing 10% fetal bovine serum, serving as a chemoattractant. After incubation for 24 hours, migrated cells on the underside of the membrane were fixed in methanol for 10 minutes and stained with 0.1% crystal violet for 30 minutes, followed by 3–5 washes with PBS. Stained cells were visualized under a microscope, with random fields selected for analysis. All experiments were conducted in quintuplicate.

Immunofluorescence

MDA-MB-231 and SUM159PT cells were placed on coverslips and cultured overnight. Following 24 hours of treatment with NE and SGJPF, the cells were washed twice with PBS and fixed with 4% paraformaldehyde for 15 minutes. After fixation, they were permeabilized with 0.5% Triton X-100 for 20 minutes, followed by blocking with QuickBlock™ Blocking Buffer for Immunol Staining. The coverslips were then incubated overnight at 4°C with primary antibodies against p-SRC and Vimentin. The next day, secondary antibodies were applied at room temperature for 1 hour. Finally, DAPI was used to stain the nuclei before imaging. All experiments were conducted in quintuplicate.

Western Blot Analysis

Cells and tissues were lysed in RIPA lysis buffer supplemented with 1% protease and phosphatase inhibitor cocktail I to extract total protein. Protein concentrations were determined using the BCA protein assay kit (P0012, Beyotime Biotechnology, China). Equal amounts of protein samples were separated on 10% SDS-PAGE gels and transferred onto PVDF membranes via electrophoresis. Membranes were blocked with 5% skim milk for 1 hour, followed by overnight incubation at 4°C with primary antibodies (diluted 1:1000). On the next day, membranes were washed with TBST for 3 times (each for 10 minutes), and then incubated with secondary antibodies (diluted 1:5000–1:10000) at room temperature for 1 hour. Protein bands were detected using the ECL reagent and analyzed with a chemiluminescence Western blot detection system (Tanon, China).

Phospho-Src (Tyr416) (CST; cat. #6943), Src (CST; cat. #2109), Phospho-Stat3 (Tyr705) (CST; cat. #9145), Stat3 (CST; cat. #9139), p44/42 mitogen-activated protein kinase (MAPK) (Erk1/2) (CST; cat. #4695), Phospho-p44/42 MAPK (Erk1/2) (Thr202/Tyr204) (CST; cat. #4370), Plk1 (208G4) (CST; cat. #4513), Skp2 (CST; cat. #2652), VEGFA (Proteintech; cat. #19003-1-AP), Vimentin (Proteintech; cat. #10366-1-AP), E-Cadherin (Proteintech; cat. #20874-1-AP), N-Cadherin (Proteintech; cat. #22018-1-AP), Bax (Proteintech; cat. #50599-2-Ig), Bcl2 (Proteintech; cat. #68103-1-Ig), Caspase-3 (CST; cat. #9662), Caspase-9 (CST; cat. #9502), Vinculin (CST; cat. #66305-1-Ig) were used for Western blot.

Tumor Xenograft Models and Drug Administration

All animal experimental procedures were approved by the Experimental Animal Ethics Committee of Jining No.1 People's Hospital (No. JNRM-2024-DW-088) and were conducted in accordance with the guidelines for the care and use of laboratory animals issued by the National Institutes of Health.

BALB/C nude female mice, aged 5 weeks and weighing an average of 20.0±5.0 g, were sourced from Pengyue Laboratory Animal Breeding Co., LTD. (Jinan, China). These mice were maintained under specific pathogen-free (SPF) conditions and acclimated to the facility for 1 week prior to experimentation.

The CPS modeling scheme referred to the published literature,^{21,22} and was slightly adjusted on this basis. The mice were put in the cycle of light and dark for 12h:12h (turn on the light at 7:00 in the morning), and the mice can get water and food freely at room temperature of 25 °C. Mice were randomly assigned to either the control group (n=5) or the

experimental group (n=15). The experimental group was exposed to unpredictable stressors, while the control group did not experience stress. See [Supplementary Table 2](#) for the specific process of stress stimulation in the experimental group. On the 28th day after these stress stimuli, behavioral assessments, including tail suspension test and forced swim test were conducted to evaluate whether the animals had obvious CPS symptoms. Then, on the 2nd day, the xenograft TNBC mouse model was established by subcutaneously injecting 3×10^7 MDA-MB-231 cells/mL (200 μ L per mouse) into the right axillary region following anesthesia with 3% isoflurane.

Starting from the 32nd day, the mice in the experimental group continued to experience stressors in accordance with the established protocol until the end of the study. On the 35th day, the experimental mice were randomly assigned to three groups: the model group, the low-dose SGJPF group (SGJPF-L), and the high-dose SGJPF group (SGJPF-H). Mice in the SGJPF-L group received SGJPF at 10 g/kg, while the SGJPF-H group were administered 30 g/kg, with the model group receiving an equivalent volume of normal saline. After 25 consecutive days of treatment, the mice were sacrificed, and the tumors were excised, weighed, photographed, and preserved for further analysis.

Tissue Histology and Immunostaining

After euthanasia, tissues were harvested, and preserved in 4% paraformaldehyde, then embedded in paraffin, and sectioned into 5 μ m slices. Subsequently, tissue slices were deparaffinized, rehydrated, and subjected to hematoxylin-eosin (HE) and immunohistochemistry staining as per the specific instructions. Images were acquired under a light microscope.

Statistical Analysis

Data were derived from a minimum of 5 independent replicates and are expressed as mean \pm SD. For comparisons involving multiple groups, one-way ANOVA was performed. Statistical significance was defined as $p < 0.05$.

Results

Main Substances of SGJPF

The identification of SGJPF components was obtained through HPLC/MS analysis. As illustrated in [Supplementary Figure 1](#), the total ion chromatogram (TIC) of SGJPF identification displays the overall abundance of all ions at specific time points. Initial data sorting was conducted using CD2.1 (Thermo Fisher), followed by a comprehensive search and comparison within the mzCloud database. A total of 806 compounds were identified in mzCloud. Detailed structural information for compounds with an mzCloud Best Match score of ≥ 60 is provided in [Supplementary Table 3](#). The main components include flavonoids, polyphenols, saponins, polysaccharides, alkaloids, terpenoids, coumarins, organic acids, and glycosides.

Network Pharmacology Analysis

The number of SGJPF active ingredients meeting the filtering condition was 406, and then 1274 corresponding targets of them were identified. Data mining of the GEO database revealed 2431 differently expressed genes (DEG), which were regarded as TNBC-related genes ([Figure 2A](#) and [B](#)). Additionally, 880 genes related to CPS were harvested. On the basis of the above three data sets, 32 common genes were finally screened out, which were regarded as the action target of SGJPF in the treatment of TNBC complicated with CPS ([Figure 2C](#)).

After using the ClusterProfiler package for GO functional analysis, 853 biological processes (BP), 24 cell components (CC), and 42 molecular functions (MF) were enriched. The top 6 remarkably enriched terms of BP, CC and MF were shown in [Figure 2D](#) and [E](#). KEGG enrichment analysis of the therapeutic targets identified 56 enriched pathways, with key involvement in pathways including “chemical carcinogenesis-receptor activation”, “hepatitis B”, and “Kaposi sarcoma-associated herpesvirus infection”. ([Figure 2F](#)).

PPI network of 32 targets was created by Cytoscape software, in which the nodes with larger size and darker color were near the center and of great importance ([Figure 3A](#)). To further screen the core targets, the LASSO regression analysis as well as the Cytohubba and MCODE plugins of the Cytoscape were adopted ([Figure 3B–E](#)). The results

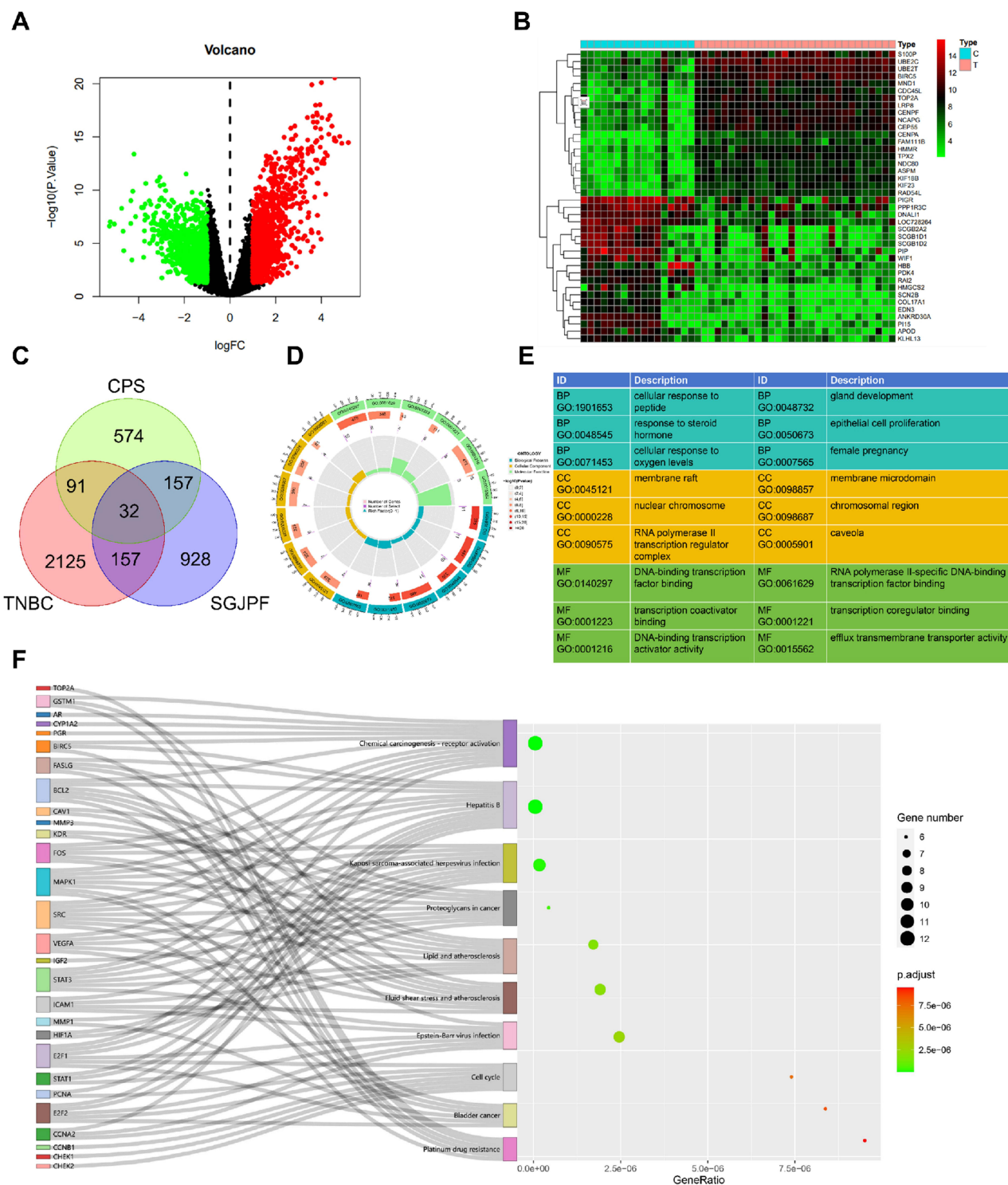


Figure 2 Therapeutic targets of SGJPF for CPS-related TNBC. **(A and B)** The volcano plot and the heatmap of the DEG in TNBC. **(C)** The Venn diagram showing the therapeutic targets of SGJPF for CPS-related TNBC. **(D and E)** GO enrichment analysis and top 6 terms. **(F)** KEGG enrichment analysis.

showed that 10, 5, and 11 targets were filtered out respectively, and their common targets were SRC, ERK and STAT3 (Figure 3F).

In the end, we conducted virtual molecular docking between these targets and paeoniflorin through Autodock software to verify their binding potential. The results indicated binding energies of -7.01 kcal/mol for paeoniflorin

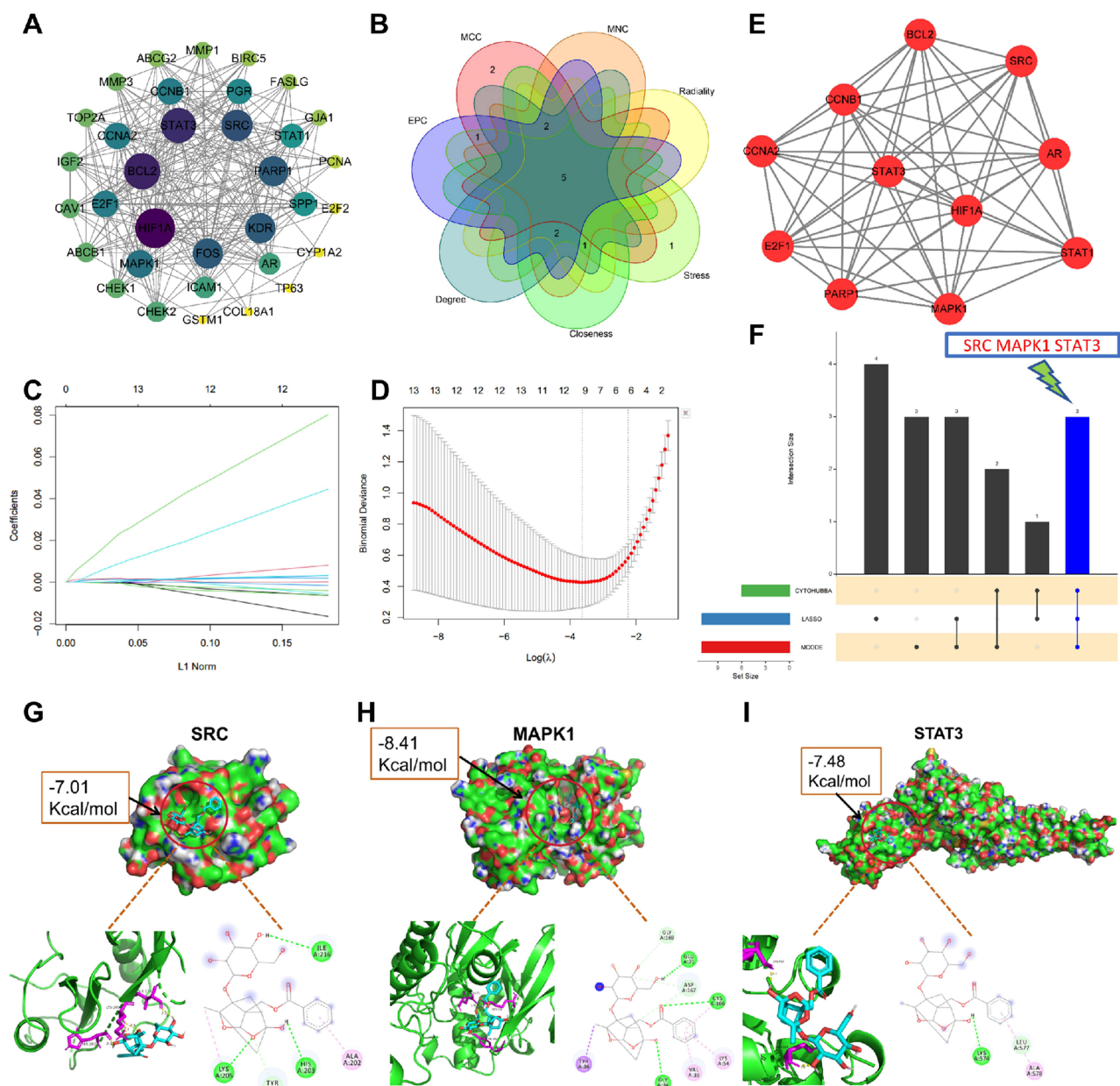


Figure 3 The screening of core targets. **(A)** PPI network of 32 therapeutic targets. **(B–F)** The key targets screened from CytosHubba plugin **(B)**, LASSO regression analysis **(C and D)**, and MCODE plugin **(E)**, respectively. **(F)** The core targets ultimately identified. **(G–I)** Molecular docking of paeniflorin with the core targets SRC, MAPK1, and STAT3.

with SRC, -8.41 kcal/mol with MAPK1, and -7.48 kcal/mol with STAT3 (Figure 3G–I). According to relevant reports, a binding energy of less than -7 kcal/mol between a ligand and receptor indicates strong binding potential.²³ Therefore, our docking results indicated that paeniflorin can be closely connected with SRC, MAPK1, and STAT3 in structural conformations, which indirectly indicated the reliability of our network pharmacological prediction results.

SGJPF Inhibited TNBC Cell Viability

Initially, we employed varying concentrations of NE (0, 1, 5 and 10 μ M) to stimulate MDA-MB-231 and SUM159PT cells, aiming to closely replicate the cellular conditions of breast cancer under CPS *in vitro*. The colony-forming assay and Edu staining results confirmed the attainment of the desired effect, identifying 10 μ M as the optimal NE intervention concentration (Figure 4A–C, I, J and Supplementary Figure 2A and B).

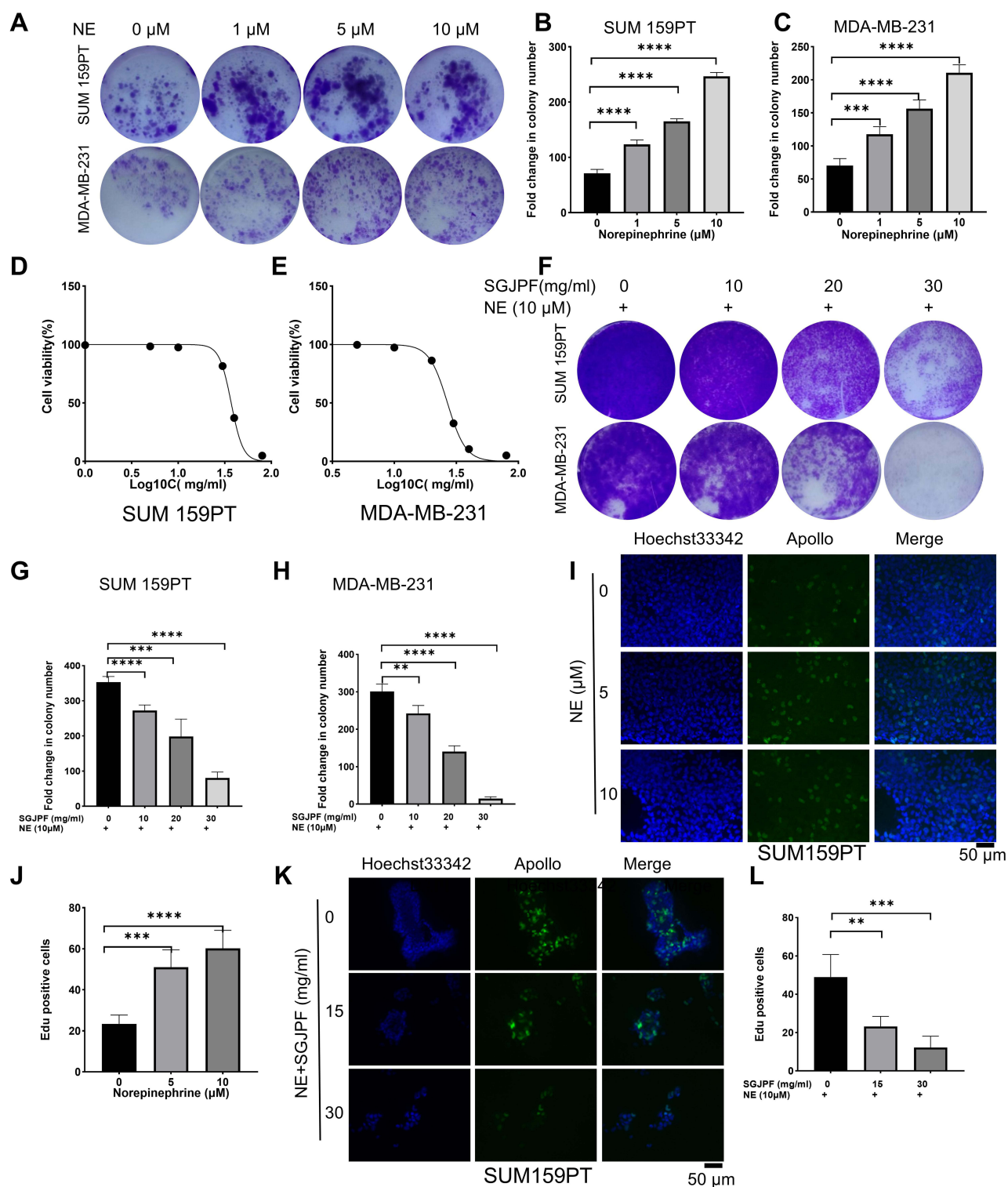


Figure 4 SGJPF reversed the enhanced proliferation caused by NE stimulation. (**A–C**) Colony formation assay showing NE could augment the proliferative effects of MDA-MB-231 and SUM159PT cells. ($n=5$). $***p < 0.001$, $****p < 0.0001$. (**D** and **E**) MDA-MB-231 and SUM159PT cells were treated with varying concentrations of SGJPF for 24 hours prior to being subjected to the CCK-8 assay. (**F–H**) Colony formation assay showing SGJPF inhibited the NE-enhanced proliferation of MDA-MB-231 and SUM159PT cells in a dose-dependent manner. ($n=5$). $*p < 0.01$, $**p < 0.001$, $****p < 0.0001$. (**I** and **J**) EdU assay was conducted following 24 hours of stimulation with different concentrations of NE in SUM159PT cells. DNA replication activities were visualized in green, and nuclei were counterstained with Hoechst 33342 (blue). ($n=5$). $***p < 0.001$, $****p < 0.0001$. (**K** and **L**) EdU assay showing SGJPF inhibited the NE-induced proliferation of SUM159PT cells in a dose-dependent manner. ($n=5$). $*p < 0.01$, $***p < 0.001$.

To investigate the effects of SGJPF on the viability and morphology of MDA-MB-231 and SUM159PT cells, the cells were exposed to varying concentrations of SGJPF for 24 hours. Colony formation assays demonstrated a dose-dependent inhibition of TNBC cell growth by SGJPF (Figure 4F–H). Specifically, treatment with 20 mg/mL and 30 mg/mL of SGJPF for 24 hours significantly reduced cell viability. At 30 mg/mL, survival rates of SUM159PT and MDA-MB-231 cells decreased to 19% and 7.5%, respectively. The IC₅₀ values of SGJPF under NE stimulation were calculated as 26 mg/mL for MDA-MB-231 cells and 37 mg/mL for SUM159PT cells (Figure 4D and E). In summary, SGJPF markedly inhibited the proliferation of both cell lines, as further confirmed by EdU staining (Figure 4K, L and Supplementary Figure 2C and D).

SGJPF Inhibited the Invasion and Migration of TNBC Cells

Similar to the method described above, varying concentrations of NE (0, 1, 5 and 10 μ M) were employed to stimulate MDA-MB-231 and SUM159PT cells, thereby closely replicating the cellular conditions of breast cancer under CPS. The results from the wound-healing and transwell invasion assays confirmed the desired outcome, establishing 10 μ M as the optimal concentration for NE intervention (Supplementary Figure 3A–J).

As illustrated in Figure 5A and B, after 24 hours of SGJPF treatment, the wound closure percentages for the SUM159PT cell line were 33%, 54%, 94%, and 97%, respectively, across increasing concentrations of SGJPF. Similarly, the wound closure percentages for MDA-MB-231 cells were 24%, 73%, 82%, and 95% under the same conditions (Figure 5C and D). SGJPF effectively inhibited the migration of both MDA-MB-231 and SUM159PT cells *in vitro*. Compared to the initial time point (0 h), SGJPF treatment led to a marked, dose-dependent decrease in cell migration (Figure 5E–G), indicating that SGJPF suppresses TNBC cell migration in a dose-dependent fashion. Notably, the inhibitory effect of SGJPF (30 mg/mL) treatment group was similar to that of dasatinib (100 nm) treatment group (Figure 5A–D).

Further, as shown in Figure 5H–J, in NE-pretreated (10 μ M) SUM159PT and MDA-MB-231 cells, SGJPF treatment significantly reduced the number of cells migrating through the chamber (blue-purple spots), with the inhibitory effect increasing alongside drug concentration. These findings demonstrate that SGJPF suppresses TNBC cell invasion in a dose-dependent manner.

SGJPF Induced Apoptosis of TNBC Cells

The impact of SGJPF on apoptosis in 10 μ M NE-pretreated cells was analyzed by flow cytometry. The data revealed a substantial rise in apoptosis rates in MDA-MB-231 and SUM159PT cells following SGJPF treatment. In SGJPF-treated TNBC cells, the apoptosis rates increased from 2.31% to 19.29% in SUM159PT cells and from 7.12% to 22.93% in MDA-MB-231 cells, compared to the control group (Figure 6A and B). Moreover, SGJPF resulted in a marked reduction in the Bcl-2/Bax protein ratio, along with a notable increase in the cleaved caspase-9 and cleaved caspase-3 expression (Figure 6G and H).

SGJPF Induced Cell Cycle Arrest in TNBC Cells

MDA-MB-231 and SUM159PT cells pretreated with 10 μ M NE were incubated with varying concentrations of SGJPF for 24 hours and then analyzed via flow cytometry. As shown in Figure 6C and D, the G₂/M phase in MDA-MB-231 cells increased from 13% to 40%, while the S phase remained stable (12% to 10%), and the G₀/G₁ phase decreased from 79% to 48%. In SUM159PT cells, SGJPF treatment increased the G₂/M phase from 14% to 30%, the S phase from 19% to 45%, and decreased the G₀/G₁ phase from 67% to 24%. These findings indicate that SGJPF induces G₂/M phase cell cycle arrest in both cell lines.

Furthermore, as illustrated in Figure 6E–H, Plk1 and Skp2 protein levels were upregulated in NE-treated TNBC cells but were significantly downregulated following SGJPF treatment.

SRC/ERK/STAT3 Signaling Axis Mediated the Anti-Cancer Effects of SGJPF on TNBC Cells

To assess the regulatory effect of SGJPF on TNBC, MDA-MB-231 and SUM159PT cells were first incubated with NE at concentrations of 0, 1, 5, and 10 μ M. The results demonstrated that NE stimulation led to a dose-dependent increase in

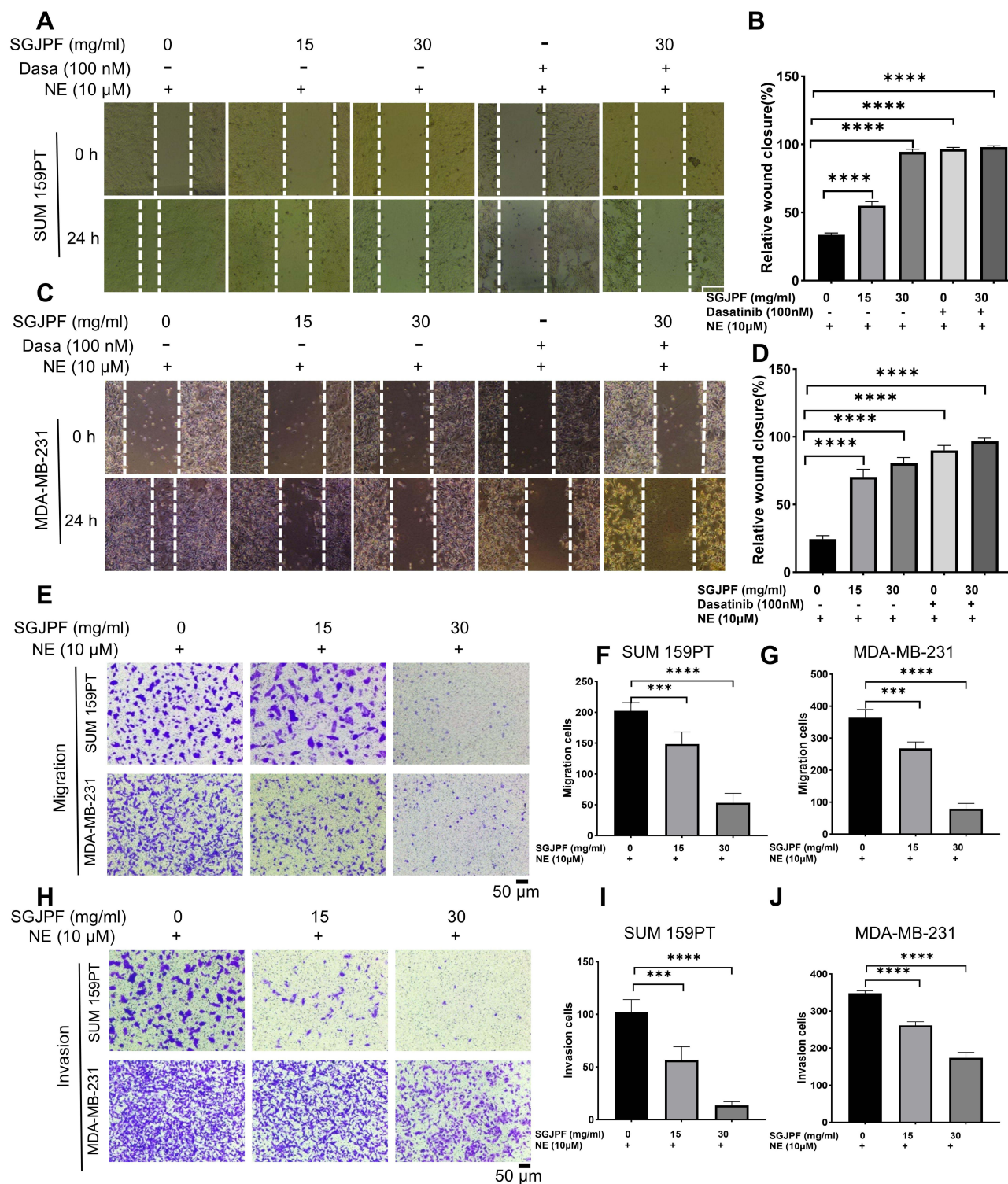


Figure 5 SGJPF inhibited the invasion and migration of TNBC cells. (A–D) Wound-healing assay was used to assess the inhibitory effect of SGJPF on the migration of NE-stimulated MDA-MB-231 and SUM159PT cells, with Dasatinib serving as a positive control. (n=5). **** $p < 0.0001$. (E–J) Transwell assay was performed to demonstrate the ability of SGJPF to inhibit both migration and invasion in NE-stimulated MDA-MB-231 and SUM159PT cells. (n=5). *** $p < 0.001$, **** $p < 0.0001$.

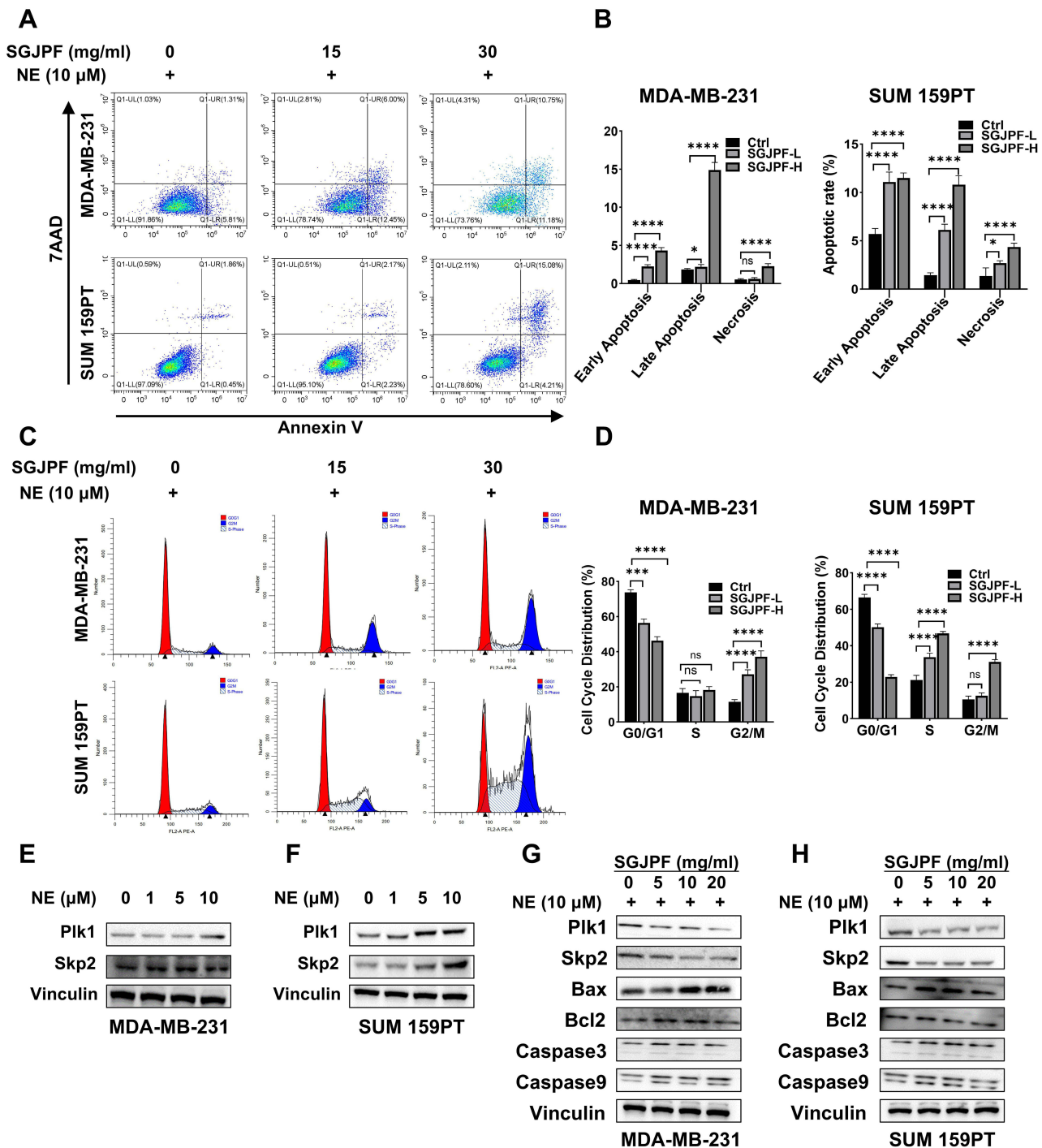


Figure 6 SGJPF induced cell apoptosis and cycle arrest. **(A and B)** After exposure to SGJPF at specified concentrations for 24 hours, MDA-MB-231 and SUM159PT cells incubated with NE were stained with Annexin V-APC/7-AAD and analyzed by flow cytometry. ($n=5$). * $p < 0.05$, **** $p < 0.0001$. **(C and D)** Cell cycle distribution was assessed in NE-incubated MDA-MB-231 and SUM159PT cells with varying concentrations of SGJPF. ($n=5$). *** $p < 0.001$, **** $p < 0.0001$. **(E and F)** NE induced the expression of cycle proteins Plk1 and Skp2 in MDA-MB-231 and SUM159PT cells. **(G and H)** SGJPF reduced the expression ratio of Bcl-2/Bax and increased the expression levels of cleaved caspase-9 and cleaved caspase-3 in MDA-MB-231 and SUM159PT cells.

the phosphorylation of SRC, STAT3, and ERK, indicating activation of these signaling pathways (Figure 7A and B). After pretreatment with 10 μ M NE, the cells were then exposed to varying concentrations of SGJPF (0, 5, 10, and 20 mg/mL) for 24 hours. As shown in Figure 7C and D, SGJPF treatment reduced p-SRC, p-STAT3, and p-ERK levels in a concentration-dependent manner in both MDA-MB-231 and SUM159PT cells compared to the control. These findings

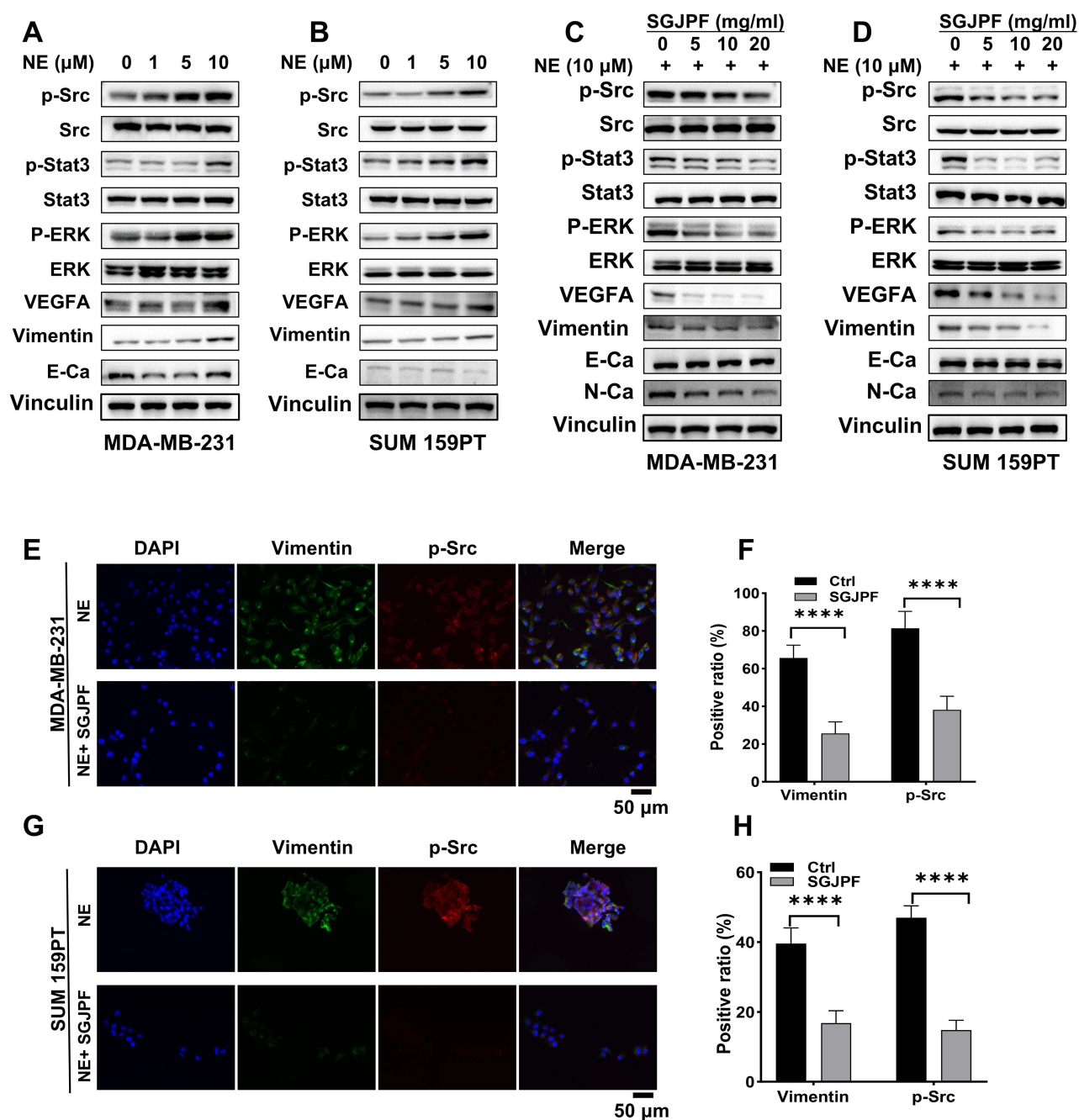


Figure 7 Effect of SGJPF on NE-induced SRC/ERK/STAT3 pathway dysregulation. (A and B) NE caused the the up-regulation of p-SRC, p-STAT3, p-ERK, VEGFA, Vimentin and down-regulation of E-Ca in MDA-MB-231 and SUM159PT cells. (C and D) SGJPF could restore the abnormal expression of related proteins caused by NE, including p-SRC, p-STAT3, p-ERK, VEGFA, N-Ca, E-Ca, and Vimentin. (E–H) IF assay showing that SGJPF could attenuate the increase of Vimentin and p-SRC proteins expression caused by NE. (n=5). *** $p < 0.001$, **** $p < 0.0001$.

were further corroborated by immunofluorescence results, which showed consistent trends (Figure 7E–H). SGJPF treatment effectively induced dephosphorylation of the SRC/ERK/STAT3 signaling axis in breast cancer cells.

Additionally, SGJPF counteracted NE-induced changes in key EMT markers, reversing the downregulation of E-cadherin and the upregulation of N-cadherin, VEGFA, and Vimentin (Figure 7A–D).

It was worth noting that SGJPF, as mentioned above, caused significant cell cycle arrest and apoptosis of MDA-MB-231 and SUM159PT cells under the same concentration gradient and intervention conditions, while also markedly

inhibiting cell motility and invasiveness. These findings demonstrate that the SRC/ERK/STAT3 signaling axis may mediate the anticancer effects of SGJPF in TNBC cells.

SGJPF Suppressed the Tumor Growth in TNBC Xenograft Models

Following 25 days of SGJPF intervention, the mice were euthanized subsequent to weighing, and their tumors were isolated and weighed (Figure 8A and B). The average tumor weight of the control, model, SGJPF-L, and SGJPF-H groups were 0.1g, 0.486g, 0.068g, and 0.038g, respectively (Figure 8C and D). Compared to the control group, mice in the model group, subjected to chronic stress and devoid of SGJPF treatment, exhibited a marked escalation in tumor weight and size. However, this increase was notably reversed in the SGJPF-intervention group, particularly evident in the SGJPF-H group, manifesting a striking effect. Further, *in vivo* toxicity of SGJPF at effective doses was evaluated by regular weight monitoring. Throughout the entire duration of drug administration, body weight changes in the high- and low-dose SGJPF groups remained below 5%, exhibiting no significant difference when compared with the control and model groups (Figure 8E). Histological examination of tumor sections via HE staining revealed profound alterations in both low and high dose SGJPF groups, characterized by disorganized cellular structure and nuclear karyopyknosis, while Ki-67 staining manifested SGJPF's remarkable suppression of TNBC cell proliferation (Figure 8G). The results of p-SRC, Vimentin, and CD31 staining suggested that SGJPF's therapeutic effect on TNBC may involve inhibition of tumor invasion and metastasis regulated by SRC-related signaling pathways (Figure 8G). In addition, Western blot results of tumor tissues were similar to those of *in vitro* experiments, further confirming our conclusion (Figure 8F).

Discussion

TNBC, comprising approximately 15% of all breast cancers, has a high recurrence and 5-year mortality rates. In past decades, chemotherapy regimen has historically been the preferred treatment option for TNBC, but chemotherapy has significant toxicity and side effects, and the prognosis and survival rate of patients are far from ideal.²⁴ Recently, with the use of multiple monoclonal antibody therapies, the situation has improved to some extent.²⁵ However, the overall response rate to treatments like immune checkpoint inhibitors is only 20% to 40%, and a significant number of cases have immune-related adverse reactions that can not be ignored.²⁶ The occurrence and development of cancer involve the coordinated regulation of various targets and signaling pathways. The treatment of cancer by TCM decoctions emphasizes its integrity and the synergistic use of distinct drugs, which has the characteristics of multiple action links, various pathways and numerous targets.²⁷ Therefore, TCM intervention may serve as a highly beneficial adjunct treatment for cancer, with our clinical studies demonstrating that SGJPF effectively slows TNBC progression and enhances patients' quality of life.¹⁷

Psychiatric disorders are widely recognized as predisposing factors for various diseases, particularly cancer.²⁸ Reports indicate that TNBC has a stronger association with severe mood disturbances compared to other cancer types.^{7,29} Many TNBC patients frequently experience prolonged psychological stress prior to diagnosis, with CPS being one of the most common forms. In classical TCM theory, the pathogenesis of breast cancer progression caused by CPS primarily involves "liver qi stagnation", which disrupts the flow of qi in the body.^{30,31} Liver Qi stagnation is a common pathogenesis in TCM, typically manifested by emotional disturbances such as depression, anxiety, and irritability. It is often accompanied by symptoms like chest tightness, pain in the hypochondrium, poor appetite, and insomnia. This TCM syndrome is frequently triggered by long-term emotional suppression, stress from work or life, and is considered a root cause of various diseases, including cancer.^{32–34} The main therapeutic effect of SGJPF is to smooth liver qi stagnation, relieve depression, and regulate the balance of qi flow in the body, thereby exerting anti-breast cancer effects. In the present study, to further explore the active components and mechanisms of action of SGJPF, we first identified the key components of SGJPF using LC-MS. Next, we applied network pharmacology to screen for the potential therapeutic targets and signaling pathways of SGJPF. Using the SwissTargetPrediction database, SGJPF was predicted to target 231 potential genes. After filtering through the GEO and GeneCard databases, 32 therapeutic targets related to CPS and TNBC were identified. KEGG analysis highlighted the pathway of "chemical carcinogenesis-receptor activation", involving key biological processes like cellular response to peptides, steroid hormones, and epithelial proliferation. The PPI network analysis identified SRC, MAPK1 (ERK), and STAT3 as central targets, known to drive tumor

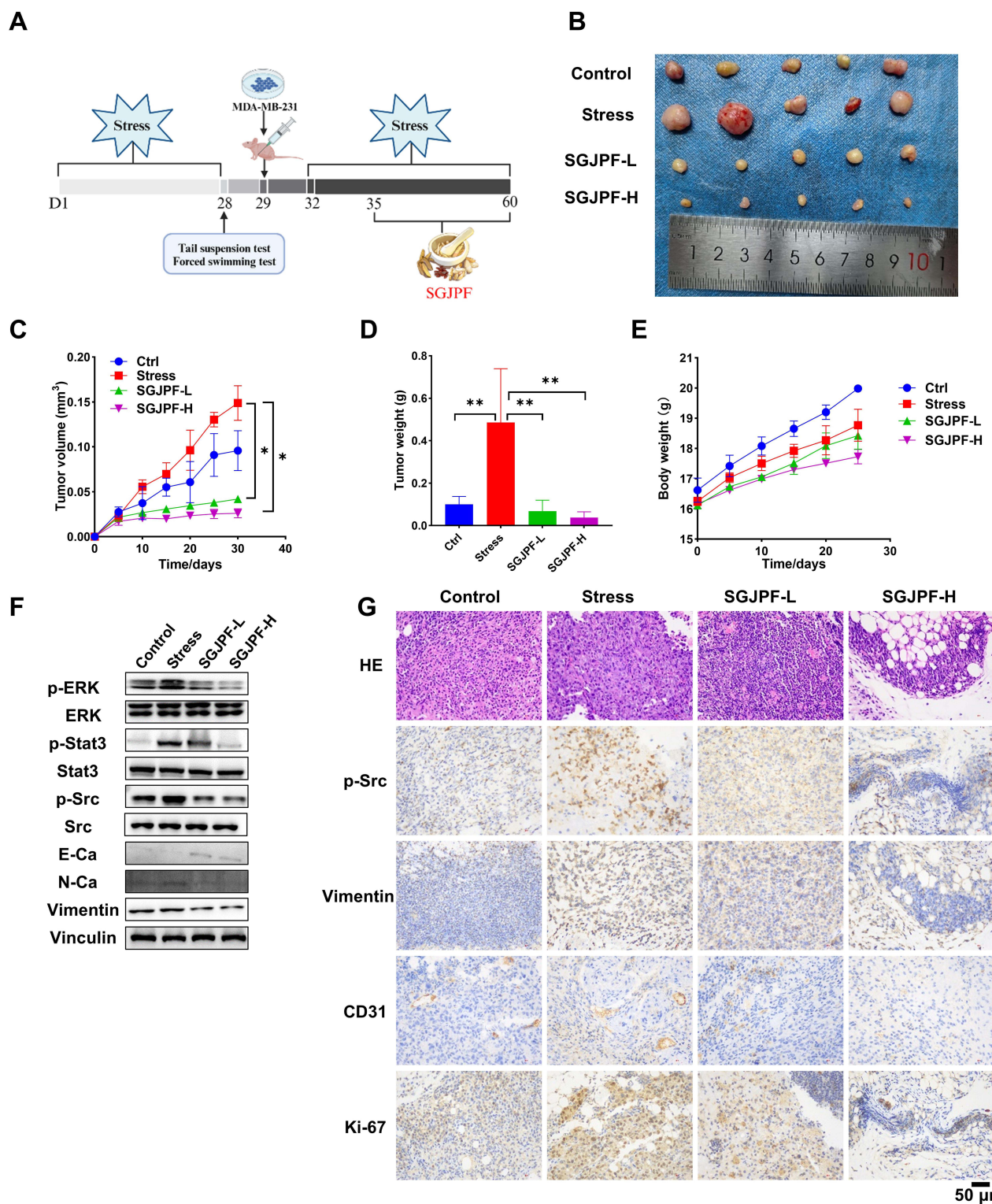


Figure 8 SGJPF intervention suppressed tumor progression in TNBC xenografted mice. **(A)** Schematic diagram of the course of SGJPF intervention in vivo. **(B)** The visual representation of the tumors in xenografted mice. **(C)** Line chart of tumor size over time. (n=5). * $p < 0.05$. **(D)** Tumor weight of different groups of mice at the end of the experiment. (n=5). ** $p < 0.01$. **(E)** Line chart of mice body weight over time. **(F)** WB showing the comparison of expression of p-Src, p-ERK, p-STAT3, E-Ca, N-Ca, and Vimentin in tumor tissues of different groups. **(G)** IHC images showing the staining of HE, p-Src, Vimentin, CD31, and Ki-67 in tumor sections from each experimental group.

proliferation, metastasis and invasion.^{35–37} Additionally, molecular docking demonstrated a strong binding affinity between these targets and paeoniflorin, a primary active ingredient of SGJPF. Based on the above findings, it was plausible to speculate that these three core targets may play a key role in the treatment of CPS-related TNBC with SGJPF.

Under the action of CPS, the sympathetic nervous system (SNS) usually has abnormal activation, which is one of the main reasons for the growth, progression and metastasis of breast cancer.³⁸ The activation of SNS is mainly mediated by catecholamines such as NE, and further acts on the TME, including promoting angiogenesis, stimulating tumor cell proliferation and survival, and exacerbating the deterioration of inflammatory networks.^{39,40} In view of this, we added NE to mimic a model simulating breast cancer cells in CPS state for further biological research. This construction method has been repeatedly shown to be feasible in the studies of breast cancer comorbid with chronic stress state.^{41,42} Initially, we optimized the CPS-like conditions using NE at 10 μ M, which effectively simulated the breast cancer cellular environment. Under these conditions, SGJPF significantly suppressed cell viability in a dose-dependent manner, as confirmed by colony-forming assays and EdU staining. Notably, SGJPF at 30 mg/mL decreased the survival of MDA-MB-231 and SUM159PT cells to 7.5% and 19%, respectively, demonstrating a profound cytotoxic effect. Further, SGJPF induced apoptosis in TNBC cells, as evidenced by increased apoptotic markers and a reduced Bcl-2/Bax ratio. This was accompanied by G2/M phase cell cycle arrest, underscoring SGJPF's ability to disrupt cell cycle progression. Furthermore, SGJPF displayed potent anti-migratory and anti-invasive properties, as wound healing and transwell assays showed significant inhibition of TNBC cell motility. This suppression was associated with the modulation of EMT markers, where SGJPF reversed NE-induced changes in E-cadherin, N-cadherin, VEGFA, and Vimentin expression. In vivo studies corroborated the in vitro findings, where SGJPF treatment in TNBC xenograft models markedly suppressed tumor growth. Mice treated with high-dose SGJPF exhibited a significant decrease in tumor weight and size without notable toxicity. Histological examination further supported these results, with reduced Ki-67 expression and impaired tumor architecture observed in SGJPF groups. These findings reinforce the therapeutic potential of SGJPF in targeting CPS-related TNBC through multiple mechanisms, including inhibition of proliferation, migration and invasion. Indeed, several TCM formulations, particularly those aimed at smoothing liver qi stagnation or promoting detoxification, have been reported to exert significant anti-breast cancer effects.^{30,31} Jin'gan Capsules specifically inhibited cell growth in various breast cancer cell lines, including MDA-MB-231, MDA-MB-468, and MCF-7,³¹ highlighting their potential as an effective therapeutic approach for breast cancer treatment.

Mechanistically, we verified that the SRC/ERK/STAT3 signaling axis mediates the anti-cancer effects of SGJPF on TNBC cells. Western blot results revealed that MDA-MB-231 and SUM159PT cells, when pretreated with 10 μ M NE and subsequently exposed to varying concentrations of SGJPF (0, 5, 10, and 20 mg/mL) for 24 hours, exhibited a significant decrease in phosphorylated SRC (p-SRC), STAT3 (p-STAT3), and ERK (p-ERK) levels. The findings were corroborated by immunofluorescence results, confirming that SGJPF induces dephosphorylation of the SRC/ERK/STAT3 signaling axis. These results align with previous studies highlighting the pivotal role of the SRC/ERK/STAT3 pathway in cancer cell proliferation, survival, and metastasis.^{43–45} The dephosphorylation observed suggests an inhibition of this pathway, consistent with SGJPF's impact on cell cycle arrest and apoptosis. The significant cell cycle arrest and apoptosis in MDA-MB-231 and SUM159PT cells, alongside the reduced motility and invasiveness under SGJPF treatment, further emphasize the therapeutic potential of SGJPF against TNBC. Notably, the SRC/ERK/STAT3 axis is crucial for regulating genes involved in cell cycle progression and survival, where phosphorylated SRC activates ERK, or directly phosphorylates STAT3, driving oncogene transcription.^{46,47} The observed inhibition of this signaling cascade by SGJPF underscores its role in disrupting critical cellular processes in TNBC cells. Moreover, the differential sensitivity of TNBC cells to SGJPF highlights the importance of signaling context in mediating drug response. Previous research has shown that targeting the SRC/ERK/STAT3 pathway can synergize with other therapeutic strategies to enhance anti-tumor efficacy.⁴⁸ Multiple inhibitors directed against SRC, ERK, or STAT3 have demonstrated promising potential in both clinical trials or preclinical studies for the treatment of TNBC.^{49–51} Collectively, the findings of this study offer strong support for further exploration of SGJPF as a complementary therapeutic option in the management of TNBC.

Conclusions

In conclusion, this study highlights the significant potential of SGJPF as an effective therapeutic strategy for TNBC. SGJPF was shown to inhibit TNBC cell proliferation and induce apoptosis, and G2/M cell cycle arrest in vitro. These effects were supported by in vivo experiments, which demonstrated reduced tumor growth and altered expression of key signaling proteins. Furthermore, network pharmacology and molecular docking analyses suggested that SGJPF may exert its effects, at least in part, by modulating the SRC/ERK/STAT3 signaling pathway. Together, these findings provide a mechanistic framework and experimental basis for further investigation of SGJPF in the treatment of TNBC.

Abbreviations

TNBC, triple negative breast cancer; CPS, chronic psychological stress; SGJPF, Shugan Jianpi Formula; NE, norepinephrine; TCM, traditional Chinese medicine; CAMD, computer-aided molecular design; HE, hematoxylin-eosin; IHC, immunohistochemistry; IF, immunofluorescence; WB, Western blotting; PVDF, polyvinyl difluoride; DEG, differentially expressed gene; Dasa, dasatinib; BP, biological processes; CC, cell components; MF, molecular functions; SNS, sympathetic nervous system; BDNF, brain-derived neurotrophic factor; HR, hazard ratio.

Acknowledgments

This research was supported by the National Natural Science Foundation of China (NSFC) (Nos. 82074360), the Shandong Provincial Natural Science Foundation (Nos. ZR2022MH319 and ZR2022LZY027), the Young Taishan Scholars Program of Shandong Province (No. tsqn201909200), the Shandong Postdoctoral Science Foundation (No. SDCX-ZG-202302036), the Scientific and Technological Innovation Project of Medical Staff in Shandong Province (No. SDYWZGKCJHLH2023072), the Traditional Chinese Medicine Science and Technology Development Plan of Shandong Province (No. Q-2022026), the Doctoral Fund of Jining First People's Hospital (No. 2022-BS-008), project of National Administration of Traditional Chinese Medicine (GZY-KIS-SD-2023-026), and the Key Research and Development Program of Jining City (grant no. 2023YXNS223 and 2022YXNS170).

Author Contributions

All authors made a significant contribution to the work reported, whether that is in the conception, study design, execution, acquisition of data, analysis and interpretation, or in all these areas; took part in drafting, revising or critically reviewing the article; gave final approval of the version to be published; have agreed on the journal to which the article has been submitted; and agree to be accountable for all aspects of the work.

Disclosure

The authors have declared that no competing interest exists for this work.

References

- Lukasiewicz S, Czezelewski M, Forma A, Baj J, Sitarz R, Stanislawek A. Breast cancer-epidemiology, risk factors, classification, prognostic markers, and current treatment strategies-an updated review. *Cancers*. 2021;13(17). doi:10.3390/cancers13174287
- Liang Y, Zhang H, Song X, Yang Q. Metastatic heterogeneity of breast cancer: molecular mechanism and potential therapeutic targets. *Semin Cancer Biol*. 2020;60:14–27. doi:10.1016/j.semcancer.2019.08.012
- Li Y, Zhang H, Merkher Y, et al. Recent advances in therapeutic strategies for triple-negative breast cancer. *J Hematol Oncol*. 2022;15(1):121. doi:10.1186/s13045-022-01341-0
- Ingram SH, De Roos AJ, Wallace RB, et al. Influence of occupational stress on breast cancer incidence in the Women's Health Initiative. *Health Psychol*. 2025;44(4):335–344. doi:10.1037/hea0001437
- Ochoa-Arnedo C, Prats C, Travier N, et al. Stressful life events and distress in breast cancer: a 5-years follow-up. *Int J Clin Health Psychol*. 2022;22(2):100303. doi:10.1016/j.ijchp.2022.100303
- Falcinelli M, Thaker PH, Lutgendorf SK, Conzen SD, Flaherty RL, Flint MS. The role of psychologic stress in cancer initiation: clinical relevance and potential molecular mechanisms. *Cancer Res*. 2021;81(20):5131–5140. doi:10.1158/0008-5472.CAN-21-0684
- Lillberg K, Verkasalo PK, Kaprio J, Teppo L, Helenius H, Koskenvuo M. Stressful life events and risk of breast cancer in 10,808 women: a cohort study. *Am J Epidemiol*. 2003;157(5):415–423. doi:10.1093/aje/kwg002
- Helgesson O, Cabrera C, Lapidus L, Bengtsson C, Lissner L. Self-reported stress levels predict subsequent breast cancer in a cohort of Swedish women. *Eur J Cancer Prev*. 2003;12(5):377–381. doi:10.1097/00008469-200310000-00006

9. Qiu J, Shen Z, Jiang G, Ni Q. Isoproterenol-induced upregulation of hsp accelerates triple-negative breast cancer cell proliferation and migration through enhancing the transcriptional activity of HIF-1 α . *Anticancer Agents Med Chem.* 2023;23(4):470–477. doi:10.2174/1871520622666220817125817
10. Liu LY, Feng B, Chen J, et al. Herbal medicine for hospitalized patients with severe depressive episode: a retrospective controlled study. *J Affect Disord.* 2015;170:71–77. doi:10.1016/j.jad.2014.08.027
11. Wang J, Wu Q, Ou C, Lu G, Yu H. Research on Xiaoyao Powder in the treatment of depression based on epigenetics and quality markers. *Front Neurosci.* 2023;17:1223451. doi:10.3389/fnins.2023.1223451
12. Wei Q, Jing Z, Zhi-Ye H. Evaluation of Danzhi Xiaoyao powder and amlodipine sustained-release tablets in follow-up treatment of the hypertensive crisis and the interleukin-6 gene expression. *Cell Mol Biol.* 2021;67(2):166–170. doi:10.14715/cmb/2021.67.2.26
13. Zhu YL, Li SL, Zhu CY, Wang W, Zuo WF, Qiu XJ. Metabolomics analysis of the antidepressant prescription Danzhi Xiaoyao powder in a rat model of chronic unpredictable mild stress (CUMS). *J Ethnopharmacol.* 2020;260:112832. doi:10.1016/j.jep.2020.112832
14. Zhang Y, Luo Y, Hou X, et al. Xiaoyao powder alleviates the hippocampal neuron damage in chronic unpredictable mild stress-induced depression model rats in hippocampus via connexin 43Cx43/glucocorticoid receptor/brain-derived neurotrophic factor signaling pathway. *Bioengineered.* 2022;13(1):383–394. doi:10.1080/21655979.2021.2005744
15. He M, Li L, Wei X, et al. Xiaoyao powder improves endometrial receptivity via VEGFR-2-mediated angiogenesis through the activation of the JNK and P38 signaling pathways. *J Ethnopharmacol.* 2022;282:114580. doi:10.1016/j.jep.2021.114580
16. Yang Y, Wang Y, Wang T, Jiang X, Wang L. Screening active components of modified Xiaoyao powder as NRF2 agonists. *Cell Biochem Funct.* 2017;35(8):518–526. doi:10.1002/cbf.3309
17. Wang LF, Ji H, Wang Y, Zhao H, Jiang S. Clinical observation of the therapeutic effect of Shugan Jianpi formula combined with chemotherapy in the treatment of advanced triple-negative breast cancer. *World J Trad Chin Western Med.* 2020;15(05):932–935. doi:10.13935/j.cnki.sjzx.200534
18. Talevi A. Computational approaches for innovative antiepileptic drug discovery. *Expert Opin Drug Discov.* 2016;11(10):1001–1016. doi:10.1080/17460441.2016.1216965
19. Gao Y, Ji W, Lu M, et al. Systemic pharmacological verification of Guizhi Fuling decoction in treating endometriosis-associated pain. *J Ethnopharmacol.* 2022;297:115540. doi:10.1016/j.jep.2022.115540
20. Wei M, Li H, Li Q, et al. Based on network pharmacology to explore the molecular targets and mechanisms of gegen Qinlian decoction for the treatment of ulcerative colitis. *Biomed Res Int.* 2020;2020(1):5217405. doi:10.1155/2020/5217405
21. Yang F, Liu Y, Chen S, et al. A GABAergic neural circuit in the ventromedial hypothalamus mediates chronic stress-induced bone loss. *J Clin Invest.* 2020;130(12):6539–6554. doi:10.1172/JCI136105
22. Burstein O, Doron R. The unpredictable chronic mild stress protocol for inducing anhedonia in mice. *J Vis Exp.* 2018;(140). doi:10.3791/58184
23. Shi S, Sun M, Liu Y, Jiang J, Li F. Insight into Shenqi Jiangtang Granule on the improved insulin sensitivity by integrating in silico and in vivo approaches. *J Ethnopharmacol.* 2022;282:114672. doi:10.1016/j.jep.2021.114672
24. Chaudhuri A, Kumar DN, Dehari D, et al. Endorsement of TNBC biomarkers in precision therapy by nanotechnology. *Cancers.* 2023;15(9):2661. doi:10.3390/cancers15092661
25. Khadela A, Soni S, Shah AC, et al. Unveiling the antibody-drug conjugates portfolio in battling triple-negative breast cancer: therapeutic trends and future horizon. *Med Oncol.* 2022;40(1):25. doi:10.1007/s12032-022-01884-9
26. Keenan TE, Tolaney SM. Role of immunotherapy in triple-negative breast cancer. *J Natl Compr Canc Netw.* 2020;18(4):479–489. doi:10.6004/jnccn.2020.7554
27. Wang S, Long S, Deng Z, Wu W. Positive role of Chinese herbal medicine in cancer immune regulation. *Am J Chin Med.* 2020;48(7):1577–1592. doi:10.1142/S0192415X20500780
28. Grassi L. Psychiatric and psychosocial implications in cancer care: the agenda of psycho-oncology. *Epidemiol Psychiatr Sci.* 2020;29:e89. doi:10.1017/S2045796019000829
29. Von Ah D, Kang DH. Correlates of mood disturbance in women with breast cancer: patterns over time. *J Adv Nurs.* 2008;61(6):676–689. doi:10.1111/j.1365-2648.2007.04563.x
30. Hu L, Yang Y, Wang Z, Wen C, Cheng X. A real-world data analysis-based study of Chinese medicine treatment patterns after breast cancer surgery. *Medicine.* 2023;102(50):e36642. doi:10.1097/MD.00000000000036642
31. Qiu J, Zhang Z, Hu A, et al. Integrating UPLC-HR-MS/MS, network pharmacology, and experimental validation to uncover the mechanisms of jin'gan capsules against breast cancer. *ACS Omega.* 2022;7(32):28003–28015. doi:10.1021/acsomega.2c01921
32. Chen GF, Mao MC, Yu CC, et al. Near-infrared brain imaging study of depressive disorder with liver qi stagnation syndrome before and after treatment. *Front Psychiatry.* 2025;16:1529575. doi:10.3389/fpsy.2025.1529575
33. Lin H, Zhang X, Zheng Y, Tang C, Wang J. Research on the soothing Liver - Qi stagnation method in the treatment of postoperative papillary thyroid carcinoma patients' concomitant depression: a randomized controlled clinical trial. *Medicine.* 2024;103(37):e39325. doi:10.1097/MD.00000000000039325
34. Wu Q, Yan H, Kang Z. A review of traditional Chinese medicine for triple negative breast cancer and the pharmacological mechanisms. *Am J Chin Med.* 2024;52(4):987–1011. doi:10.1142/S0192415X2450040X
35. Amanchy R, Zhong J, Hong R, et al. Identification of c-Src tyrosine kinase substrates in platelet-derived growth factor receptor signaling. *Mol Oncol.* 2009;3(5–6):439–450. doi:10.1016/j.molonc.2009.07.001
36. Ullah R, Yin Q, Snell AH, Wan L. RAF-MEK-ERK pathway in cancer evolution and treatment. *Semin Cancer Biol.* 2022;85:123–154. doi:10.1016/j.semcancer.2021.05.010
37. Siersbaek R, Scabia V, Nagarajan S, et al. IL6/STAT3 signaling hijacks estrogen receptor alpha enhancers to drive breast cancer metastasis. *Cancer Cell.* 2020;38(3):412–423e9. doi:10.1016/j.ccell.2020.06.007
38. Chen X, Wang M, Yu K, et al. Chronic stress-induced immune dysregulation in breast cancer: implications of psychosocial factors. *J Transl Int Med.* 2023;11(3):226–233. doi:10.2478/jtim-2021-0050
39. Wang C, Shen Y, Ni J, Hu W, Yang Y. Effect of chronic stress on tumorigenesis and development. *Cell Mol Life Sci.* 2022;79(9):485. doi:10.1007/s00018-022-04455-3
40. Sousa DM, Fernandes V, Lourenco C, et al. Profiling the adrenergic system in breast cancer and the development of metastasis. *Cancers.* 2022;14(22):5518. doi:10.3390/cancers14225518

41. Park HJ, Lee SC, Park SH. Norepinephrine stimulates M2 macrophage polarization via beta2-adrenergic receptor-mediated IL-6 production in breast cancer cells. *Biochem Biophys Res Commun.* 2024;741:151087. doi:10.1016/j.bbrc.2024.151087
42. Liu J, Chai XX, Qiu XR, et al. Type X collagen knockdown inactivate ITGB1/PI3K/AKT to suppress chronic unpredictable mild stress-stimulated triple-negative breast cancer progression. *Int J Biol Macromol.* 2024;273(Pt 1):133074. doi:10.1016/j.ijbiomac.2024.133074
43. Raji L, Tetteh A, Amin A. Role of c-Src in carcinogenesis and drug resistance. *Cancers.* 2023;16(1):32. doi:10.3390/cancers16010032
44. Guo YJ, Pan WW, Liu SB, Shen ZF, Xu Y, Hu LL. ERK/MAPK signalling pathway and tumorigenesis. *Exp Ther Med.* 2020;19(3):1997–2007. doi:10.3892/etm.2020.8454
45. Dinakar YH, Kumar H, Mudavath SL, Jain R, Ajmeer R, Jain V. Role of STAT3 in the initiation, progression, proliferation and metastasis of breast cancer and strategies to deliver JAK and STAT3 inhibitors. *Life Sci.* 2022;309:120996. doi:10.1016/j.lfs.2022.120996
46. Ni CW, Hsieh HJ, Chao YJ, Wang DL. Shear flow attenuates serum-induced STAT3 activation in endothelial cells. *J Biol Chem.* 2003;278(22):19702–19708. doi:10.1074/jbc.M300893200
47. Hu X, Wu X, Xu J, Zhou J, Han X, Guo J. Src kinase up-regulates the ERK cascade through inactivation of protein phosphatase 2A following cerebral ischemia. *BMC Neurosci.* 2009;10(1):74. doi:10.1186/1471-2202-10-74
48. Kong Q, Ma M, Zhang L, et al. Icariside II potentiates the anti-PD-1 antitumor effect by reducing chemotactic infiltration of myeloid-derived suppressor cells into the tumor microenvironment via ROS-mediated inactivation of the SRC/ERK/STAT3 signaling pathways. *Phytomedicine.* 2023;110:154638. doi:10.1016/j.phymed.2022.154638
49. Sun Y, Lin X, Aske JC, et al. Dasatinib attenuates overexpression of Src signaling induced by the combination treatment of veliparib plus carboplatin in triple-negative breast cancer. *Cancer Chemother Pharmacol.* 2019;84(6):1241–1256. doi:10.1007/s00280-019-03962-8
50. Zhong Y, Deng L, Shi S, et al. The novel STAT3 inhibitor WZ-2-033 causes regression of human triple-negative breast cancer and gastric cancer xenografts. *Acta Pharmacol Sin.* 2022;43(4):1013–1023. doi:10.1038/s41401-021-00718-0
51. Prasath V, Boutrid H, Wesolowski R, et al. Phase II study of MEK inhibitor trametinib alone and in combination with AKT inhibitor GSK2141795/uprosertib in patients with metastatic triple negative breast cancer. *Breast Cancer Res Treat.* 2025;210(1):179–189. doi:10.1007/s10549-024-07551-z

Drug Design, Development and Therapy

Publish your work in this journal

Drug Design, Development and Therapy is an international, peer-reviewed open-access journal that spans the spectrum of drug design and development through to clinical applications. Clinical outcomes, patient safety, and programs for the development and effective, safe, and sustained use of medicines are a feature of the journal, which has also been accepted for indexing on PubMed Central. The manuscript management system is completely online and includes a very quick and fair peer-review system, which is all easy to use. Visit <http://www.dovepress.com/testimonials.php> to read real quotes from published authors.

Submit your manuscript here: <https://www.dovepress.com/drug-design-development-and-therapy-journal>

Dovepress
Taylor & Francis Group